

HYBRID MULTIPHASE CFD SIMULATION FOR LIQUID-LIQUID INTERFACIAL AREA PREDICTION IN ANNULAR CENTRIFUGAL CONTACTORS

Kent E. Wardle

Chemical Sciences and Engineering Division, Argonne National Laboratory, Argonne, IL 60439, U.S.A., kwardle@anl.gov

A hybrid multiphase CFD solver which combines the Eulerian multi-fluid method with VOF sharp interface capturing has been developed for application to annular centrifugal contactors. This solver has been extended to enable prediction of mean droplet size and liquid-liquid interfacial area through a single moment population balance method. Simulations of liquid-liquid mixing in a simplified geometry and a model annular centrifugal contactor are reported with droplet breakup/coalescence models being calibrated versus available experimental data. Quantitative comparison is made for two different housing vane geometries and it is found that the predicted droplet size is significantly smaller for vane geometries which result in higher annular liquid holdup.

I. INTRODUCTION

This work is part of an overall effort with the goal of delivering computational tools for detailed simulation of liquid-liquid extraction unit operations aimed to provide a pathway for prediction of key operational performance measures (e.g. stage efficiency, other phase carry-over (back-mixing)) for any given set of conditions. Such predictive capability will help inform process-level modeling tools as well as deliver insight into unit design and operation. To accomplish this, methods are required which can adequately predict liquid-liquid mixing and interfacial area generation as well as the formation and transport of small droplets.

Liquid-liquid contacting equipment used in solvent extraction processes has the dual purpose of mixing and separating two immiscible fluids. Consequently, such devices inherently encompass a wide variety of multiphase flow regimes from segregated to dispersed flow types and present unique challenges to traditionally flow regime-dependent multiphase computational fluid dynamics (CFD) methods. In order to meet these needs, a hybrid multiphase CFD tool was recently developed (Ref. 1) which combines multiple methodologies to enable simulation of flows spanning both dispersed and segregated regimes as encountered in these devices.

Of the equipment types generally used for solvent extraction processing of used nuclear fuel, centrifugal contactors have the largest relative knowledge gap and at the same time the greatest opportunity for significant benefits to a future fuel cycle facility due to their compact size and efficient

operation. In such devices (Figure 1), the flows of the two immiscible liquid phases enter a narrow annulus between a stationary cylindrical housing and a rotating inner cylinder. The mixture flows down under the rotor where radially-oriented vanes attached to the stationary housing direct it into the hollow rotor in which the two phases are separated by centrifugal action according to their disparate densities.

A thorough review of CFD modeling efforts to date for annular centrifugal contactors (also called annular centrifugal ‘extractors’) has recently been published by Vedantam et al. (Ref. 2). The hybrid multiphase coupling methodology applied and extended here is of particular importance to capture both the liquid-liquid dispersion flow as well as the complex, dynamic fluid-rotor interaction in the mixing zone (Ref. 3). Wardle and Weller (Ref. 1) set forth the details of the foundational computational methodology of the hybrid multiphase solver and its application to liquid-liquid extraction flows. This paper presents ongoing work to extend this solver for dispersed phase droplet size and interfacial area prediction using a reduced order population balance method.

II. COMPUTATIONAL METHODS

II.A. Hybrid Multiphase Solver

Only a general overview of the hybrid multiphase flow simulation methodology will be given here as the details are reported elsewhere (Ref. 1). On top of the framework of an N -phase Eulerian multi-fluid solution framework (one momentum equation for each phase with interphase momentum coupling terms), a Volume Of Fluid (VOF) style sharp interface capturing algorithm is applied for desired phase pairs. This is done through addition of interface compression to the volume fraction transport equations and the use of limiters to maintain boundedness of phase fractions and their sum. A variety of drag correlations and schemes are available for interphase momentum coupling as well as surface tension forces when in sharp interface conditions. This solver has been developed using the open-source CFD toolkit OpenFOAM, and has been included in the version 2.1 release of OpenFOAM as `multiphaseEulerFoam`.

While only a constant droplet diameter model is included in the basic solver, the droplet diameter access functions have been implemented as a C++ library such that variable diameter models can be easily implemented. As out-

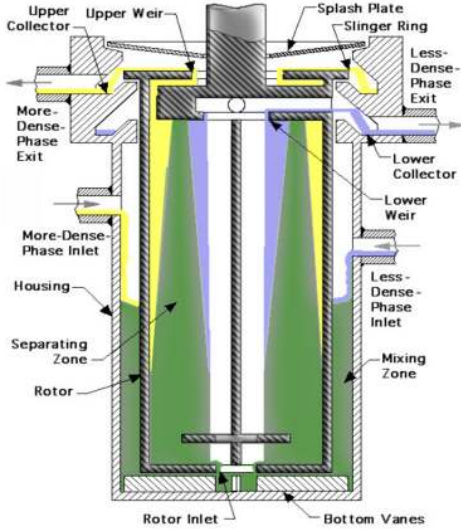


Figure 1. Sketch of an annular centrifugal contactor.

lined in the following sections, we have further expanded on the solver to include capability for variable droplet size and interfacial area prediction.

II.B. Droplet Size Capturing Using a Reduced Population Balance Model

A next step in this work aimed at ultimately predicting solute extraction efficiency is accurate prediction of inter-phase mixing, dispersed phase droplet size, and liquid–liquid interfacial area. A few different methods are available for interfacial area prediction including population balances, interfacial area transport, and Lagrangian methods—the last being applied primarily to liquid sprays where a finite number of droplets exist and it is feasible to track each in a discrete manner. For a broad range of multiphase flows, population balance methods are the most commonly used.

A range of solution methods for varying levels of detail and complexity have been developed for capture of the droplet size distribution function. All of these methods rely on underlying models for droplet breakup and coalescence to drive the evolution of the droplet size based on the local flow conditions (typically via the turbulence dissipation rate ε). The sheer number of available models and model variations (see (Ref. 4) or (Ref. 5) for a review of breakup models and (Ref. 6) for coalescence models) shows the challenge of developing general models which are transferable among various multiphase systems; consequently, the major uncertainty for population balance methods lies in the fidelity of the underlying breakup/coalescence models. For these reasons, it was chosen to implement a reduced-complexity population balance method based on the work of Attarakih et al. (Ref. 7) and the implementation set forth by Drumm and

co-workers (Ref. 8). Using this as the basis, a variety of droplet breakup and coalescence models can be implemented and tested versus experimental data to determine the most appropriate models for the present application. In this way solver development and computational efforts are focused on the areas of greatest uncertainty.

The method of Attarakih et al. (Ref. 7) considers only a single moment of the droplet distribution and thus reduces the population balance down to two quantities: the total number (or number density) and the total volume. Since the volume fraction equation for the dispersed phase is already solved only one additional transport equation is required thus limiting the additional computational burden. The particle number density N_d is related to the particle mean mass diameter d_{30} according to:

$$d_{30} = \sqrt[3]{\frac{6\alpha_d}{\pi N_d}} \quad (1)$$

The transport equation for N_d is given by:

$$\frac{\partial(\rho_d N_d)}{\partial t} + \nabla \cdot [\rho_d \vec{u}_d(d_{30}) N_d] = \rho_d S \quad (2)$$

where the source term S is a straightforward function of the droplet size-dependent breakage (g) and aggregation (a) rates:

$$S = [n_d - 1]g(d_{30})N_d - \frac{1}{2}a(d_{30}, d_{30})N_d^2 \quad (3)$$

The solver code for the population balance model has been implemented as an expandable C++ library such that any number of different breakup and coalescence models can be implemented and selected independently at runtime. Following the efforts of Drumm and coworkers (Ref. 9) who evaluated several models for simulation of a rotating disc liquid–liquid contactor, a mixed model was initially employed in which the breakup model used was that of Martinez-Bazan et al. (Ref. 10) given by:

$$g(d) = \frac{\kappa \sqrt{\beta_0 (\varepsilon d)^{2/3} - 12(\sigma/\rho d)}}{d} \quad (4)$$

$$\kappa = 0.25 \quad (5)$$

$$\beta_0 = 8.2 \quad (6)$$

and the coalescence model was from Prince and Blanch (Ref. 11) where the coalescence rate (a) is taken as the product of two terms: the collision frequency (h) and coalescence efficiency λ .

$$a(d_1, d_2) = h(d_1, d_2) \cdot \lambda(d_1, d_2) \quad (7)$$

$$h(d_1, d_2) = 0.089\pi(d_1 + d_2)^2 \varepsilon^{1/3} \left(d_1^{2/3} + d_2^{2/3} \right)^{1/2} \quad (8)$$

$$\lambda(d_1, d_2) = \exp \left[-\frac{(d_1 d_2 / (4(d_1 + d_2)))^{5/6} \rho_c^{1/2} \varepsilon^{1/3}}{4\sigma^{1/2}} \ln \left(\frac{h_0}{h_c} \right) \right] \quad (9)$$

A second set of models as developed by Coulaloglou and Tavlarides (Ref. 12) has also been implemented. This model has found wide use in the literature. The breakup model for this case is given by:

$$g(d) = c_1 \frac{\varepsilon^{1/3}}{d^{2/3}(1+\phi)} \cdot \exp \left[-c_2 \frac{\sigma(1+\phi)^2}{\rho_d \varepsilon^{2/3} d^{5/3}} \right] \quad (10)$$

and the coalescence model here also is taken as the product of the collision frequency (h) and coalescence efficiency (λ) as in Equation 7:

$$h(d_1, d_2) = c_3 \frac{\varepsilon^{1/3}}{(1+\phi)} (d_1 + d_2)^2 \left(d_1^{2/3} + d_2^{2/3} \right)^{1/2} \quad (11)$$

$$\lambda(d_1, d_2) = \exp \left[-c_4 \frac{\mu_c \rho_c \varepsilon}{\sigma^2 (1+\phi)^3} \left(\frac{d_1 d_2}{d_1 + d_2} \right)^4 \right] \quad (12)$$

In this model, the constants c_1 to c_4 are termed 'universal' in the original works of Tavlarides and coworkers, however, it is clear from the many subsequent uses of this model set that these coefficients are liquid–liquid system dependent. For example, Schmidt et al. (Ref. 13) have noted additional interfacial tension (σ) dependency in the coalescence model coefficients c_3 and c_4 .

II.C. Solution Procedure

The general solution procedure for the hybrid solver including the reduced population balance model using the equations above is similar to the procedure shown in Wardle and Weller 2013 (Ref. 1). The solution of the reduced population balance model is done after solving the phase volume fractions and prior to the velocity-pressure coupling as follows:

-
1. Update d_{30} and ε
 2. Calculate breakage and coalescence rates
 3. Solve N_d transport equation 2
 4. Compute interfacial area
-

The drag coefficients used in the phase momentum equations are then computed based on the current d_{30} for dispersed phase.

Calculation of the specific interfacial area (area per unit volume) is typically done through the direct algebraic relationship with the Sauter Mean Diameter (d_{32}) of the distribution as:

$$a = 6\alpha_d/d_{32} \quad (13)$$

However, in this case we have used the mathematical moment d_{30} rather than d_{32} due to its direct relationship with

N_d . Combining Equations 1 and 13 gives the following relationship between the specific interfacial area a and the available quantities:

$$a = (d_{30}/d_{32}) d_{30}^2 \cdot \pi N_d \quad (14)$$

Thus, if the ratio of d_{30}/d_{32} can be estimated from knowledge about the shape of the distribution, the interfacial area can be determined from d_{30} and N_d locally. From experimental data of log-normal size distributions of liquid–liquid dispersions in centrifugal contactors, this value is consistently in the range of 0.75–0.80. While this clearly introduces some minor additional uncertainty to the methodology, it will be seen from data presented in later sections that this ratio does not vary significantly over the range of typical conditions. Even so, future model refinements could reduce this uncertainty through direct calculation of d_{32} in an expanded population balance implementation should the added computational cost provide commensurate benefit to predictive accuracy.

III. RESULTS AND ANALYSIS

Similar to what was done previously for the base solver, the testing of the extended solver including droplet breakup and coalescence models was done using a simplified annular mixer configuration both in 2D (axisymmetric) and 3D. The geometry of the annular model is similar to the V2 centrifugal contactor from CINC Industries in which the inner radius is 2.54 cm (2-inch rotor diameter) and the outer 3.17 cm (annular gap of 0.63 cm) and the height of the annulus is 7 cm. The top surface of the model is open to air at constant atmospheric pressure and the bottom surface is treated as a wall. A constant rotating wall velocity was applied to the rotor surface (left wall in case of 2D axisymmetric model). Turbulence was treated using Large Eddy Simulation (LES) with the Smagorinsky sub-grid model. A uniform quadrilateral mesh was used for the 2D model with spacing of 0.2 mm (32 cells across the annular gap). For the 3D model, the mesh spacing was ~ 0.4 mm (15 hexahedral cells across the annular gap, 675K cells total). Preliminary simulations for the complete mixing zone of a model CINC-V2 centrifugal contactor are presented in Section III.C. In all cases a sharp interface is maintained for the liquid–air interfaces and multi-fluid dispersed phase modeling is employed for the liquid–liquid interactions.

Recently, droplet size distribution measurements in a CINC-V2 annular centrifugal contactor having curved housing vanes were reported (Ref. 14).^{*} This work provides the only available data set of this type to date. Experiments were

^{*}The curved vanes used in (Ref. 14) are slightly different from those reported in Wardle et al. (Ref. 15) which were machined rather than cast. For the cast vanes, the vane height is constant and does not have the lower stepped region in the outer portion.

done at a total flow rate of 300 ml/min—significantly lower than typical operation—and for varying O/A ratios **less than** 1/3 (O:A, 1:3) for organic dispersed in water. Only the data for O/A = 1/3 is used here. The organic phase was polydimethylsiloxane (PDMS, $\rho = 920 \text{ kg/m}^3$, $\mu = 0.0046 \text{ Pa}\cdot\text{s}$) and the droplet size was determined through analysis of high-speed video images with a minimum identifiable diameter of ~ 40 microns. The reported interfacial tension for PDMS/water was 30 mN/m. Data was taken for rotor speeds ranging from 1100 to 3000 RPM. These data have obvious limitations (low flow rate, organic dispersed only, curved vanes only resulting in relatively low annular liquid height) which make the conditions less than ideal for equipment performance, yet they provide a preliminary means of experimental comparison and identification of major areas for breakup and coalescence model refinement. Figure 2 shows a plot of the size distributions at several rotor speeds for O/A = 0.333.

The values for the mean diameter (peak in distribution) are reported along with the Sauter mean diameter (d_{32}) and d_{30} which can be calculated from the distributions by:

$$d_{32} = \frac{\sum N_i d_i^3}{\sum N_i d_i^2} \quad (15)$$

$$d_{30} = \sqrt[3]{\frac{\sum N_i d_i^3}{N_{tot}}} \quad (16)$$

where N_i is the number of droplets observed having diameter d_i for discrete size bin i .

III.A. General Flow Characteristics: 2D & 3D Annular Mixer

Simulations were started from rest with stratified liquid–liquid layers of water (3 cm) and PDMS (1 cm) for a total liquid height of 4 cm. This starting height was somewhat arbitrarily selected as height data were not initially provided by Wyatt et al. (though the data was later provided by private communication and is included in the published paper (Ref. 14)). Simulations were run to 3 s after startup at the desired rotor speed. It was observed that the volume-averaged mean droplet diameter reach its steady-state value after approximately 1 s from startup (Figure 3). There was some variation observed in the average d_{30} corresponding to temporospatial variations in liquid–rotor contact and resultant mixing intensity. That said, in general there was little periodicity seen for any rotor speeds in the 2D geometry. For the 3D case, the overall liquid height exhibits a strong oscillatory behavior at 3000 RPM similar to what has been reported previously (Ref. 3), (Ref. 16). This liquid height oscillation translates directly into oscillations in d_{30} (Figure 4) For comparison with experiments, the mean and standard deviation of the

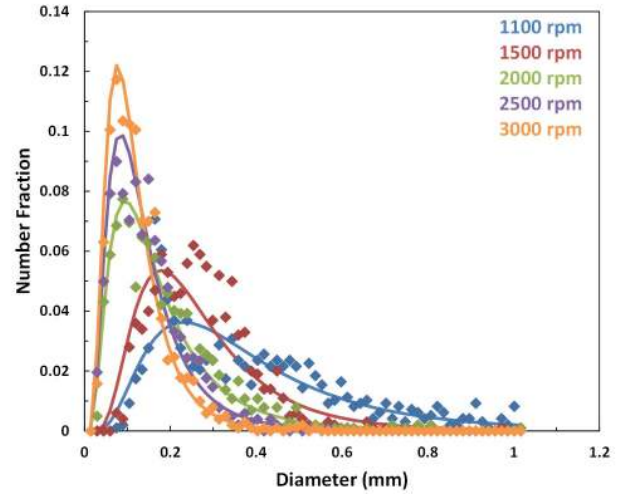


Figure 2. Droplet size distribution data from Wyatt et al. (Ref. 14) for PDMS dispersed in water in a CINC-V2 at an O/A of 0.333.

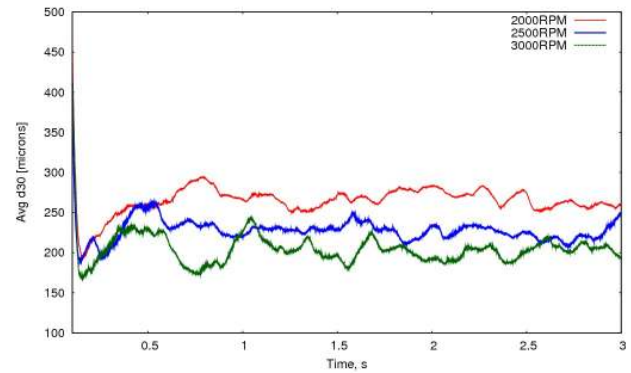


Figure 3. Time evolution of liquid volume-averaged d_{30} at three different rotor speeds in the 2D model. Results are for the Coualoglou and Tavlarides model with parameters given later in Eq. 17.

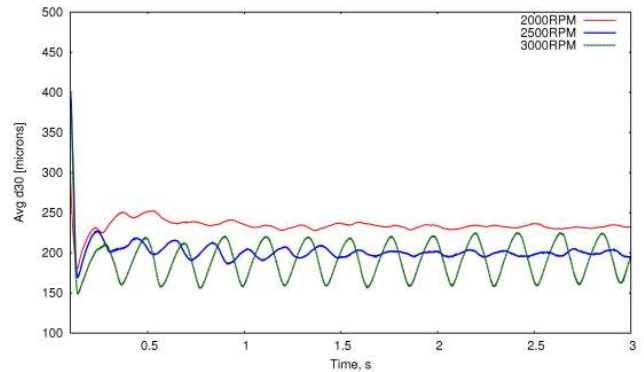


Figure 4. Time evolution of liquid volume-averaged d_{30} in the 3D model. Results are for the Coualoglou and Tavlarides model with parameters given later in Eq. 17.

liquid volume-averaged d_{30} was computed over one second of flow from $t = 2$ s to 3 s.

Figure 5 shows a snapshot of the final phase distributions (alphas), d_{30} , specific interfacial area, and histograms of the spatial distribution of d_{30} over the entire liquid volume (top right) and over the small boxed region (lower right) for the 2500 RPM case. The latter was done to determine if the general distribution over time at this location (which corresponded to the approximate height above the rotor bottom for experimental observations) differed significantly from the overall distribution. The total liquid volume-averaged values are reported in the tables in the next section. The snapshot in Figure 5 is characteristic of the general distributions observed during the transient runs. It can be seen that there was a generally stable vortex at the bottom of the domain characterized by a clock-wise rotating light-phase rich region (red color). It was observed that this vortex would occasionally get transported axially upward and remnants of other vortices can be identified by the organic-rich regions further up the liquid height. Note that the droplet size distributions observed in the experiments of Wyatt et al. (Figure 2) were found to be log-normal—the distributions seen in Figure 5 are spatial distribution of the mean droplet size (d_{30}) and therefore not expected to be directly comparable although it was seen that these also tended to be slightly log-normal. As can be expected, the smallest droplets, and consequently the largest interfacial area, are seen where/when the liquid hits the spinning rotor.

Figure 6 shows snapshots of d_{30} at three different times corresponding to successive min/max/min in liquid height (see Figure 4) for the 3D annular mixer geometry at 3000 RPM. In general, it was observed that the dispersed phase was more uniformly distributed in the 3D case as compared to 2D such that there were no temporally stable organic-rich regions. It was noted that just prior to the liquid surface dropping down and re-instigating broad contact with the rotor, that there was some modest ‘coalescence’ of the dispersed phase (both in terms of spatial phase distribution and slight drop size increase) into the beginnings of an organic-rich band near the bottom of the domain reminiscent of the behavior seen in Figure 5 except that these phase-rich regions are quickly dispersed upon substantial contact with the rotor such as in the minimum height images in Figure 6(left, right).

III.B. Quantitative Comparison of Predicted Droplet Size

Table I shows a comparison of the d_{30} (in microns) from simulations using the mixed breakup/coalescence model (MB-PB) compared with experiments and the correlations of Haas (Ref. 17). While the 3D simulations in general gave slightly lower values for d_{30} , in all cases the droplet size is

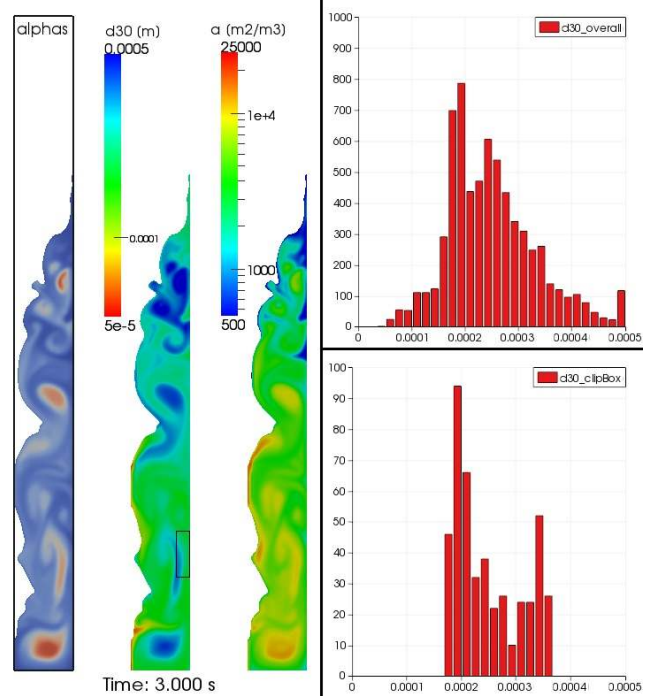


Figure 5. Snapshot of simulation data for the 2D case at 2500 RPM using the mixed MB-PB model with coalescence scaled by 0.25 (see Section III.B).

significantly over-predicted compared to experiment. To test the hypothesis that this is due to an over-prediction of coalescence, the coalescence model was turned off; the resulting values are also shown in Table I as MB-PB0. With no coalescence, the predicted droplet size is significantly smaller than the experimental values and shows much less variability (no coalescence during liquid height excursions) as shown by the smaller standard deviations. Given this observation, it was thought that simple scaling of the coalescence rate, could perhaps give a result more consistent with experiment. This is not entirely arbitrary, flows in the mixing zone of the contactor are likely to be breakup dominated—particularly given the surface active extractants used in actual chemical processes (e.g./ tributyl phosphate).

It can also be seen from the data in Table I that the ratio of d_{30}/d_{32} for the three rotor speeds included here is quite constant with a mean value of 0.76 ± 0.03 —it would seem that this value can be reliably used in Equation 14 to estimate the specific interfacial area. In addition, it was reported (Wyatt, private communication) that the uncertainty in individual droplet diameter measurements for repeated trials was approximately 10 pixels. Through propagation of error into Equations 15 and 16 the uncertainty in values for d_{32} and d_{30} are 6 and 1.2 microns, respectively. Note that the +/- values shown in Table I and II for the simulation values are the standard deviations of the temporal variation over the averaging

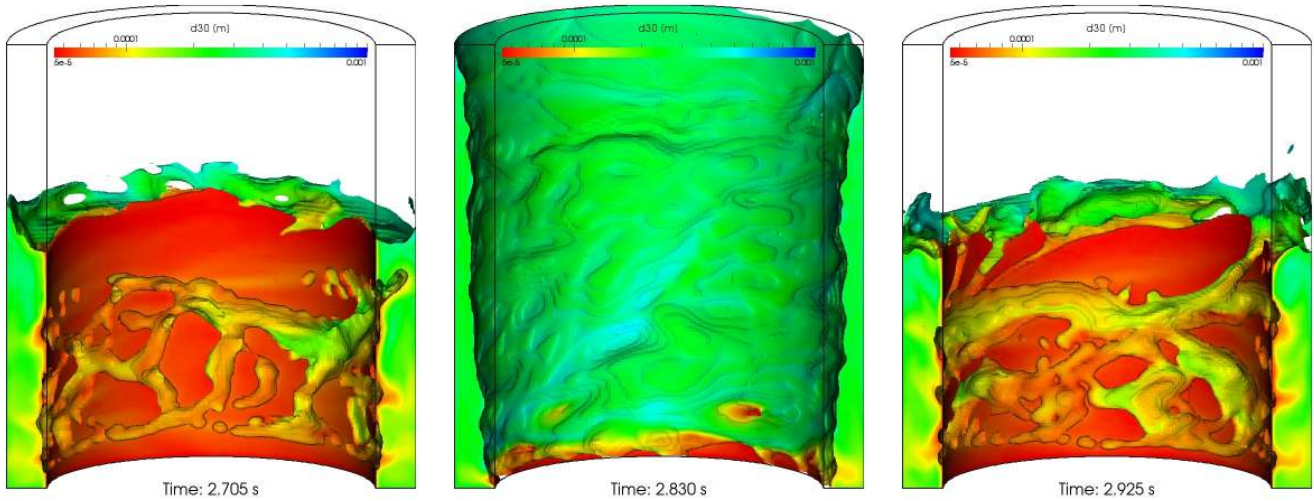


Figure 6. Snapshots of d_{30} in the 3D annular mixer model at 3000 RPM showing liquid height oscillations.

Table I. Comparison of d_{30} droplet size (microns) from 2D and 3D simulation results using Martinez-Bazan/Prince-Blanch mixed breakup/coalescence model with (MB-PB) and without (MP-PB0) coalescence versus data (Ref. 14) and correlation of Haas (Ref. 17).

RPM	MB-PB		MB-PB0		Experiment [Wyatt et al.]				Correl. (Ref. 17)
	2D	3D	2D	3D	d_{mean}	d_{32}	d_{30}	d_{30}/d_{32}	" d_{mean} "
2000	374 ± 6	343 ± 3	111 ± 2	90 ± 0	150	361	261	0.72	563
2500	-	-	-	-	120	242	190	0.79	403
3000	355 ± 10	325 ± 48	68 ± 2	68 ± 3	100	214	165	0.77	307

time period.

Table II gives the predicted values for the case where the mixed model was scaled by a factor of 0.25 (imposed coalescence rate was 25% of model value) showing improved accuracy compared to experimental values though the decrease in drop size with rotor speed was slightly underpredicted. Simulations were also done using the breakup/coalescence models of Coualoglou and Tavlarides (Ref. 12). Several variations of the constants c_1 through c_4 were tested (2D simulations only) and it was found that the values used by Azizi and Al Taweel (Ref. 18) for constants c_1 , c_2 , and c_3 , while taking c_4 from the work of Schmidt et al. (Ref. 13) gave the best match to experiments. The values used for the model of Coualoglou and Tavlarides (CT) as given in Eq. 17 were thus:

$$\begin{aligned}
 c_1 &= 0.86, \\
 c_2 &= 4.1, \\
 c_3 &= 0.04, \\
 c_4 &= 1.6 \times 10^{11} [m^{-2}]
 \end{aligned} \tag{17}$$

The results from this parameter set are also given above in Table II as CT-A123-S4. As shown in the table, this parameter set and model combination give predictions which are in the same range overall as those from the mixed model

with scaled coalescence and are slightly better at capturing the decreasing trend with higher rotor speed. There is some justification for selection of these parameters: Azizi and Al Taweel (Ref. 18) note that their parameters are optimized for cases where local variation in ε is being fully captured such as is done here with the CFD simulations using spatially resolved LES. On the other hand, Schmidt et al. (Ref. 13) report that a larger value for c_4 is required for systems with higher interfacial tension. Their system of toluene/water had a interfacial tension of 36 mN/m which is comparable to the value of 30 mN/m for the PDMS/water system.

III.C. Contactor Mixing Zone

While some general inferences can be made by comparison between simulations done in a simplified annular mixer geometry with those in a flowing centrifugal contactor system, it is not necessarily true that the two cases should be comparable. Preliminary simulations are presented here for the flow in a geometry modeled after the CINC-V2 mixing zone using the Coualoglou-Tavlarides model with the CT-A123-S4 parameter set (Eq. 17) from terse ‘calibration’ versus the available experimental data as shown above.

Simulations were conducted at a rotor speed of 2000 RPM only and were done for two different geometry

Table II. Comparison of d_{30} droplet size (microns) from 2D and 3D simulation results using scaled Martinez-Bazan/Prince-Blanch (MB-PB025) and Coualoglou-Tavlarides using mixed coefficients (CT-A123-S4) versus data of Wyatt et al.

RPM	MB-PB025		CT-A123-S4		Exp. (Ref. 14)
	2D	3D	2D	3D	d_{30}
2000	271 ± 15	229 ± 3	266 ± 9	232 ± 2	261
2500	231 ± 10	-	224 ± 8	199 ± 3	190
3000	224 ± 19	206 ± 34	201 ± 8	187 ± 21	165

variations: eight curved housing vanes (CV) as used in the experiments and four straight vanes (4V). It has been reported previously in both simulation (Ref. 15) and experiment (Ref. 16) that the liquid hold-up in the annular region is significantly greater for the 4V case as compared to CV. These simulations were intended to determine if this difference resulted in smaller droplet sizes in the 4V case as predicted by identical model sets for the two simulations. As in the experiments, and O/A of 1:3 was simulated with a total feed flowrate of 300 ml/min. The model outlet (rotor inlet) was given a constant pressure boundary condition which was set such that the resulting liquid height was comparable to that observed in the experiments—at these conditions, liquid heights (measured from the housing base) of 2.54 cm and 5.08 cm were observed for the CV and 4V cases, respectively.[†]

The meshes for the two models were similar though the 4V mesh consisted entirely of hexahedral cells (N=1.1M) generated in Cubit 13.2 and the CV mesh (N=910K) was a 98% hexahedral, snapped mesh generated with OpenFOAM's `snappyHexMesh` utility. The CV mesh came from an initial all-hex mesh for the base geometry with no housing vanes that was generated in Cubit in which only the housing vane portion had to be snapped resulting in an overall mesh quality comparable to the all-hex 4V mesh.

Figure 7 shows side-by-side snapshots comparing the liquid flow and predicted droplet size for the two housing vane types. As in the experiments, the overall liquid level in the straight vane case is twice that of the curved vanes with the result that there is a much more significant portion of the liquid in the upper annular region and substantially greater fluid–rotor contact. This increase in mixing intensity and mixing time leads to an overall droplet size that is also significantly smaller in the 4V case.

These differences can be seen quantitatively in Table III. With the four straight vanes, the drop size is smaller by about a factor of 2 while at the same time the holdup volume is 70% greater. Given that the interfacial area increases with the square of the droplet diameter, this combination results

[†]A limited number of experiments were repeated by the Wyatt et al. Sandia National Laboratory team using a four straight vane (4V) plate supplied Argonne National Laboratory. However, at the time of writing only 4V liquid height data were available.

Table III. Comparison of predicted values (averaged over a period of 2 s) from CV and 4V mixing zone simulations.

	CV	4V
d_{30} (avg), μm	480	225
d_{30} (outlet), μm	575	290
Interfacial Area (total), cm^2	540	4800*
Volume (A O), ml	30 12	50 21
O/A Ratio (holdup)	0.40	0.42
Residence Time (A O), s	8 10	13 17

*instantaneous value

in a total interfacial area that is more than 8 times greater. This, coupled with the increase in residence time, could have a significant impact on stage efficiency in an extracting system with limiting kinetics. Interestingly, though the O/A feed flow ratio is 1/3, in both cases the predicted dispersed phase holdup is greater than this resulting in a longer residence time for the organic phase—by 25% in the CV case and 30% for 4V.

The absolute value of the predicted d_{30} for the 4V case is on par with the experimentally calibrated value (261 μm), while the CV value—the actual configuration of the experiments—is significantly larger. This is because the liquid height in the 3D annular mixer case used for model calibration was more like that of the 4V geometry. Given this discrepancy, accurate prediction of the absolute droplet size for the two cases requires model recalibration either from CV mixing zone simulations or 3D annular mixer simulations with a lower liquid height. If the relative values seen here hold true for the recalibrated models, it is estimated that the droplet size in the 4V geometry would be in the range of 125 μm compared to 261 μm for the CV configuration.

This initial analysis has been restricted to the mixing zone and it is not clear if detrimental effects would arise in separation (e.g. poor separation of smaller drops leading to increase phase carry-over) for the two different configurations—though none have been quantitatively observed in experimental investigations to date. Given this qualification, it appears that for the relatively low total flow rate used here (300 ml/min compared to the estimated maximum throughput of 2.0 L/min for this size contactor) a significant increase in liquid–liquid interfacial area could be achieved through the use of four straight vanes as compared

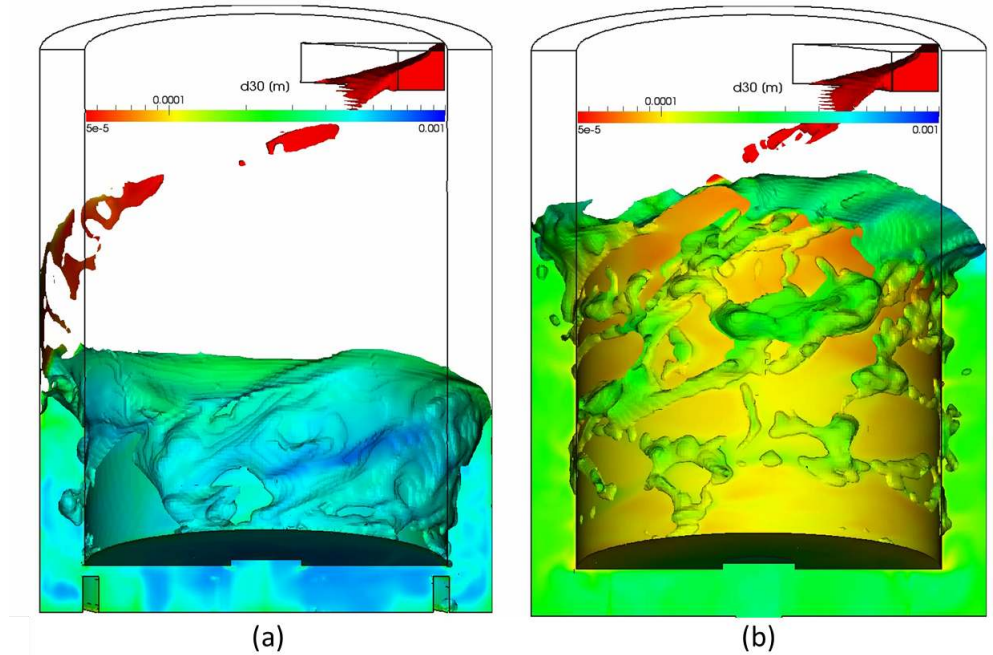


Figure 7. Snapshot comparison of flow and predicted droplet size for the (a) CV and (b) 4V geometries.

to eight curved ones.

IV. CONCLUSIONS AND FUTURE WORK

Simulations of liquid–liquid mixing in a simplified annular mixer geometry and model centrifugal contactor mixing zone have been performed providing the first ever CFD-based predictions of droplet size and interfacial area in these devices. This new simulation capability has enabled quantitative comparison of interfacial area for two different mixing vane configurations. Experiments are needed to confirm the relative decrease in drop size predicted for the 4V geometry and model/parameter selection will need to be re-evaluated based on these future results.

While it was anticipated that such would be the case, there are clearly additional, complex dependencies which are not adequately captured in the breakup/coalescence models. Consequently, it seems that regardless of which model set is used, some tuning of parameters (‘calibration’) will be required to match experimental observations. It is generally thought that breakup/coalescence parameters are phase system dependent and once calibrated for a given phase pair, should be valid over a range of conditions for that model. However, it is possible there are additional dependencies on ε from the underlying flow field. Moreover, the discrepancies in predicted droplet size relative to experiment have been mainly attributed to the need for calibration of the breakup and coalescence models, however, it is also a possibility that some portion of the error could arise from inaccurate predic-

tion of the turbulent dissipation rate ε from the LES turbulence model. Application of LES models developed in single phase flows to turbulent flows in multiphase system is an area of uncertainty among the research community in general. Future work is needed to explore the sensitivity of the simulations on turbulence SGS model selection and explore other breakup/coalescence model options. Additionally, efficient methods need to be developed for identifying optimum model parameters and confirming that these are valid over a useful range of conditions to enable direct, quantitative comparison between different equipment design options (e.g. housing vane types) and operational parameters (e.g. rotor speed).

As noted earlier, it is possible to expand the description of the droplet size distribution and enable direct computation of d_{32} through the solution of additional moments (typically 4 total, 2 more than in the reduced method). This requires additional transport equations and adds to the computational burden and implementation complexity. This would eliminate the need to assume a value for d_{30}/d_{32} in order to compute the specific interfacial area as mentioned earlier. However, this value appears to be relatively consistent and the current methodology offers a good balance of accuracy and flexibility.

V. ACKNOWLEDGMENTS

We gratefully acknowledge the use of the Fusion Linux cluster at Argonne National Laboratory and the Fission

Linux cluster at Idaho National Laboratory for computational resources. We would also like to sincerely thank Nick Wyatt of Sandia National Laboratory for providing access to their experimental data sets and for agreeing to conduct a small number of additional tests with the four straight mixing vane configuration. This work is supported by the U.S. Department of Energy, Office of Nuclear Energy under contract # DE-AC02-06CH11357.

Government License Notice This report has been created by UChicago Argonne, LLC, Operator of Argonne National Laboratory (“Argonne”). Argonne, a U.S. Department of Energy Office of Science laboratory, is operated under Contract No. DE-AC02-06CH11357. The U.S. Government retains for itself, and others acting on its behalf, a paid-up nonexclusive, irrevocable worldwide license in said article to reproduce, prepare derivative works, distribute copies to the public, and perform publicly and display publicly, by or on behalf of the Government.

REFERENCES

1. K. E. WARDLE and H. G. WELLER, “Hybrid Multiphase CFD Solver for Coupled Dispersed/Segregated Flows in Liquid-Liquid Extraction,” *Int. J. Chem. Eng.*, **2013**, 128936 (2013).
2. S. VEDANTAM, K. E. WARDLE, T. V. TAMHANE, V. V. RANADE, and J. B. JOSHI, “CFD Simulation of Annular Centrifugal Extractors,” *Int. J. Chem. Eng.*, **2012**, 759397 (2012).
3. K. E. WARDLE, T. R. ALLEN, M. H. ANDERSON, and R. E. SWANEY, “Free surface flow in the mixing zone of an annular centrifugal contactor,” *AICHE J.*, **54**, 74 (2008).
4. J. LASHERAS, C. EASTWOOD, C. MARTINEZ-BAZAN, and J. MONTANES, “A review of statistical models for the break-up of an immiscible fluid immersed into a fully developed turbulent flow,” *Int. J. Multiphase Flow*, **28**, 247 (2002).
5. Y. LIAO and D. LUCAS, “A literature review of theoretical models for drop and bubble breakup in turbulent dispersions,” *Chem. Eng. Sci.*, **64**, 3389 (2009).
6. Y. LIAO and D. LUCAS, “A literature review on mechanisms and models for the coalescence process of fluid particles,” *Chem. Eng. Sci.*, **65**, 2851 (2010).
7. M. ATTARAKIH et al., “Solution of the Population Balance Equation using the One Primary and One Secondary Particle Method (OPOSPM),” *Proc. 19th European Symposium on Computer Aided Process Engineering ESCAPE19*, 2009.
8. C. DRUMM, M. ATTARAKIH, M. W. HLAWITSCHKA, and H.-J. BART, “One-group reduced population balance model for CFD simulation of a pilot-plant extraction column,” *Ind. Eng. Chem. Res.*, **49**, 3442 (2010).
9. C. DRUMM, M. ATTARAKIH, and H.-J. BART, “Coupling of CFD with DPBM for an RDC extractor,” *Chem. Eng. Sci.*, **64**, 721 (2009).
10. C. MARTINEZ-BAZAN, J. L. MONTANES, and J. C. LASHERAS, “On the breakup of an air bubble injected into a fully developed turbulent flow. Part 1: Breakup frequency,” *J. Fluid Mech.*, **401**, 157 (1999).
11. M. J. PRINCE and H. W. BLANCH, “Bubble Coalescence and Break-up in Air-sparged Bubble Columns,” *AICHE J.*, **36**, 1485 (1990).
12. C. A. COULALOGLOU and L. L. TAVLARIDES, “Description of interaction processes in agitated liquid-liquid dispersions,” *Chem. Eng. Sci.*, **32**, 1289 (1977).
13. S. A. SCHMIDT, M. SIMON, M. M. ATTARAKIH, L. G. LAGAR, and H.-J. BART, “Droplet population balance modeling—hydrodynamics and mass transfer,” *Chem. Eng. Sci.*, **61**, 246 (2006).
14. N. B. WYATT, T. J. OHERN, and B. SHELDEN, “Drop-Size Distributions and Spatial Distributions in an Annular Centrifugal Contactor,” *AICHE J.*, DOI **10.1002/aic.14109** (published online, 2013).
15. K. E. WARDLE, T. R. ALLEN, M. H. ANDERSON, and R. E. SWANEY, “Analysis of the Effect of Mixing Vane Geometry on the Flow in an Annular Centrifugal Contactor,” *AICHE J.*, **55**, 2244 (2009).
16. K. E. WARDLE, T. R. ALLEN, M. H. ANDERSON, and R. E. SWANEY, “Experimental Study of the Hydraulic Operation of an Annular Centrifugal Contactor with Various Mixing Vane Configurations,” *AICHE J.*, **56**, 1960 (2010).
17. P. HAAS, “Turbulent Dispersion of Aqueous Drops in Organic Liquids,” *AICHE J.*, **33**, 987 (1987).
18. F. AZIZI and A. M. Al Taweel, “Turbulently flowing liquid-liquid dispersions. Part I: Drop Breakage and coalescence,” *Chem. Eng. J.*, **166**, 715 (2011).